Controlling the Directional Emission of Light by Periodic Arrays of Heterostructured Semiconductor Nanowires

Silke L. Diedenhofen,[†] Olaf T. A. Janssen,[‡] Moïra Hocevar,[§] Aurélie Pierret,[⊥,#] Erik P. A. M. Bakkers,[⊥,¶,§] H. Paul Urbach,[‡] and Jaime Gómez Rivas[*,†,¶]

[†]FOM Institute AMOLF, c/o Philips Research, High-Tech Campus 4, 5656 AE Eindhoven, The Netherlands, [‡]Optics Research Group, Delft University of Technology, PO Box 5046, 2608 GA Delft, The Netherlands, [§]Kavli Institute of Nanoscience, Quantum Transport, Delft University of Technology, 2600 GA Delft, The Netherlands, [⊥]Philips Research Laboratories, High-Tech Campus 4, 5656 AE Eindhoven, The Netherlands, and, and [¶]Applied Physics, Photonics & Semiconductor Nanophysics, Eindhoven University of Technology, 5600 MB Eindhoven, The Netherlands. [#]Present address: CEA-CNRS group "Nanophysique et semiconducteurs", INAC/SP2M, 17 rue des Martyrs, 38042 Grenoble, France.

ABSTRACT We demonstrate experimentally the directional emission of light by InAsP segments embedded in InP nanowires. The nanowires are arranged in a periodic array, forming a 2D photonic crystal slab. The directionality of the emission is interpreted in terms of the preferential decay of the photoexcited nanowires and the InAsP segments into Bloch modes of the periodic structure. By simulating the emission of arrays of nanowires with the emitting segments located at different heights, we conclude that the position of this active region strongly influences the directionality and efficiency of the emission. Our results will help to improve the design of nanowire based LEDs and single photon sources.

KEYWORDS: semiconductor nanowires · photoluminescence · photonic crystals · heterostructure · nanowire array

One of the greatest challenges of nanophotonics is to control the efficiency and directionality of the emission of light sources.[1,2] This control can be achieved by tailoring the surroundings of the sources in order to modify the optical modes into which they can decay.[3] The modification of the optical modes will allow the development of improved LEDs[4−6] and efficient single photon sources with controlled emission.[1] A very promising nanosource of radiation is semiconductor nanowires.[7−9] Recently, single nanowires have been demonstrated as nanolasers,[7] LEDs,[8] and single-photon sources.[9] The bottom-up growth process of semiconductor nanowires *via* a metal catalyst[10] facilitates the fabrication of radial and axial pn-junctions.[11−13] Because of the small lateral dimensions of nanowires, it is possible to grow defect-free heterostructures[13,14] and axial quantum dots.[15] Periodic arrays of nanowires have been fabricated, and the growth of 2D photonic crystals has been proposed[16] by defining a metal particle pattern using electron-beam lithography,[17−19] gold deposition through an anodic aluminum oxide template,[20] nanosphere lithography,[21] and nanoimprint lithography.[16,22] The capability to control the structure of single nanowires and to design arrays of nanowires with defined parameters renders these nanostructures promising for achieving full control on the emission of nanosources.

In this manuscript, we present the first experimental demonstration of the strongly modified emission of nanowires defining two-dimensional (2D) photonic crystal slabs. In particular, we show the highly directional emission of InAsP segments embedded in a periodic array of InP nanowires by measuring the angle-resolved photoluminescence. We have simulated the experimental results by finite-difference time-domain (FDTD) simulations with the use of the reciprocity theorem. Moreover, we propose that by varying the vertical position of the emitting segments the efficiency and direction of the emission can be tuned. These results set the basis for the development of light sources based on nanowires, which may improve the efficiency of LEDs and control the direction of emission of single photons, increasing the emission and detection rate in quantum optical systems.

RESULTS AND DISCUSSION

We have fabricated arrays of heterostructured InP−InAsP−InP nanowires using the vapor−liquid−solid (VLS) growth mechanism by metal−organic vapor phase epitaxy (MOVPE).[10] The VLS growth mechanism requires a metal catalyst particle. Ordered arrays of gold particles have been obtained by structuring the surface of the substrate with nanoimprint lithography.[23] The detailed

* Address correspondence to rivas@amolf.nl.

Received for review April 28, 2011 and accepted June 18, 2011.

Published online June 29, 2011
10.1021/nn201557h

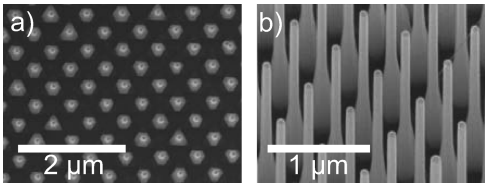

Figure 1. Scanning electron micrographs of an InP nanowire array: (a) top-view and (b) tilted-view image taken at an angle of 30°.

growth process using nanoimprint lithography is described in ref 22. Figure 1 displays scanning electron micrographs (SEM) of the array of heterostructured InP−InAsP−InP nanowires. The top-view SEM image in Figure 1a shows that the nanowires are grown in a square lattice with a pitch of 513 nm. From the tilted-view SEM image displayed in Figure 1b, the detailed structure of the nanowires is visible. The top part of the nanowires is grown straight with a diameter of 90 nm and a length of 2 μm; the bottom part is tapered with a length of 1 μm and a bottom diameter of 270 nm. Very efficient optical absorption at wavelengths shorter than the bandgap of InP, that is, 920 nm, has been recently demonstrated in these and similar arrays.[24] This absorption enables the design of nanowire based solar cells with improved light harvesting.

To have a closer look at the crystallographic structure of the nanowires and to determine both the position and the chemical composition of the InAsP segment, we performed high angle annular dark field scanning transmission electron microscopy (HAADF-STEM). Figure 2a shows a TEM image of a representative nanowire, while Figure 2b displays a TEM image with a higher magnification in which the InAsP segment is visible. The distance of the segment from the top of the nanowires is determined from three nanowires to be 1.1 ± 0.2 μm. While the InAsP segment is grown halfway through the growth time, it is not positioned in the middle of the nanowire length. This indicates that either the growth rate of InP is influenced by the presence of the InAsP segment or that the effective V/III ratio increases due to a reduction of the contribution of the substrate for the decomposition of trimethylindium (TMIn). Because of this reduced InP growth rate above the InAsP segment, the controlled fabrication of arrays of nanowires with a fixed height and an InAsP segment located at different vertical positions requires a detailed investigation of the growth mechanism. Energy dispersive X-ray spectroscopy (EDX) of the InAsP segment, shown in Figure 2c along the growth direction of the nanowire, gives an arsenic concentration of 10% in the InAsP segment and the length of the InAsP segment of 20 ± 2 nm. Figure 2d shows the photoluminescence spectrum measured at room temperature of a single nanowire excited at a wavelength of 532 nm. The emission around λ = 875 nm originates from the wurtzite InP nanowires.[25] The incorporation of As

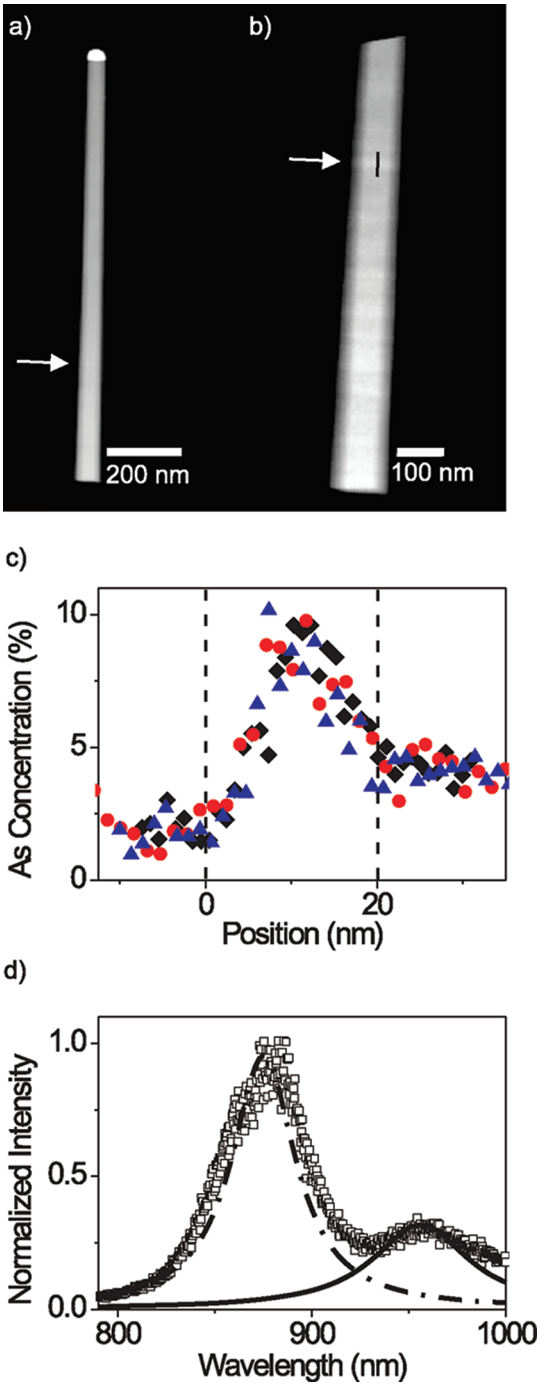

Figure 2. High angle annular dark field scanning transmission electron micrographs of an InP nanowire removed from the sample shown in Figure 1: (a) Low resolution and (b) high resolution images. The arrows indicate the position of the InAsP segment. (c) EDX linescans from three wires of the same sample indicating the As concentration along the InAsP segment. The black line in image b indicates the EDX scan line. (d) Measured photoluminescence of a single nanowire (symbols) and Lorentzian functions centered at 875 nm (dashed-dotted curve) and at 956 nm (solid curve) representing the emission spectra of the InP nanowires and InAsP segment used for the FDTD simulations.

atoms into InP leads to a narrowing of the semiconductor energy gap and to a red-shift of the photoluminescence resulting to the emission around λ = 950 nm

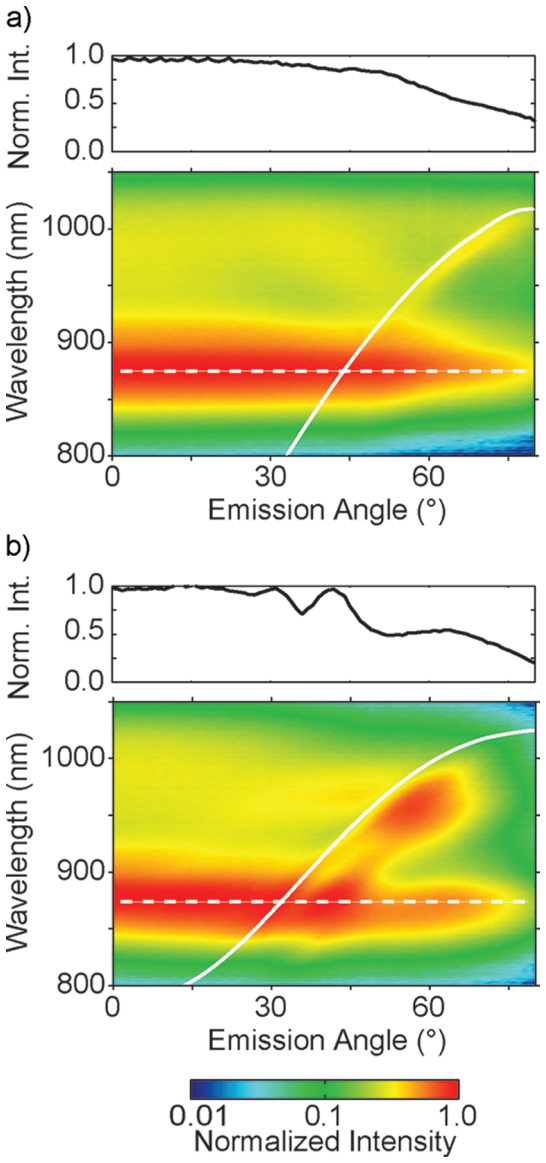

Figure 3. (a) s-polarized and (b) p-polarized photoluminescence of an array of InP nanowires normalized to the maximum photoluminescence as a function of the emission angle and wavelength. The upper insets show the normalized emission at λ = 875 nm along the white dashed lines. The white curves correspond to the calculated (a) TE Bloch mode and (b) TM Bloch mode.

from the InAsP segment. The emission of the InP nanowire and the InAsP segment can be approximated by Lorentzian functions. These Lorentzian functions are centered at λ = 875 nm with a width of 40 nm (dash-dotted curve in Figure 2d) for the emission of the InP nanowire, and at λ = 956 nm with a width of 60 nm (solid curve in Figure 2d) for the emission of the InAsP segment.

We have determined the directionality of the emission of the InP nanowires and the InAsP segments by measuring the angle-resolved photoluminescence of the array. Figure 3 panels a and b display the measurements of the photoluminescence intensity normalized to the maximum photoluminescence intensity measured normal to the sample for (a) s- and (b) p-polarization. These measurements are displayed as a function of the wavelength and the angle of detection measured from the sample normal. The upper insets show the measurements at λ = 875 nm, that is, along the dashed lines. The s-polarized emission of the nanowires at λ = 875 nm (upper inset of Figure 3a) decreases as a function of angle, following a lambertian emission profile. Some fluctuations in the photoluminescence as a function of the angle can be observed for p-polarized emission (upper inset of Figure 3b). As we show below, these oscillations are due to the periodic structure of the nanowire layer.

The most interesting feature of the photoluminescence measurements of Figure 3 is the emission of the InAsP segment (λ > 900 nm). As is apparent in Figure 3a, the s-polarized emission of the InAsP for angles between 50° and 70° shows a narrow and weak band of emission. For the p-polarized emission, there are two more intense and closely spaced bands that lead to a distinct maximum of emission around an angle of 57° and a wavelength of 956 nm.

To understand the emission of the InAsP segments, we have calculated the band structure, i.e., the Bloch modes, of a 2D photonic crystal.[26] A schematical description of the configuration of the calculation is given in Figure 4a. The 2D photonic crystal is formed by infinitely long InP (n = 3.35) nanowires with a diameter d = 90 nm and a lattice constant a = 510 nm. We have determined the transverse-electric (TE) and transverse-magnetic (TM) Bloch modes. According to Figure 4a, the TE modes have the electric field perpendicular to the nanowire elongation, that is, the y-direction, while the TM modes have the magnetic field parallel to this direction. The coupling of the TE and TM Bloch modes to s- or p-polarized free-space radiation is determined by the electromagnetic boundary conditions, which set the continuity of the field components parallel to the interface. When measuring the s-polarized emission, only the TE modes are probed. The p-polarized emission is determined by the modes having the electric field component in the z-direction, that is, TM modes. The reciprocal lattice of a square array of nanowires is given in Figure 4b, where the points of higher symmetry (Γ, X, M) delimiting the irreducible Brillouin zone are indicated. Figure 4c displays the calculated bandstructure. The black solid curves represent the TE modes, and the red dashed curves represent the TM modes. The range of our measurement is marked with the shaded region. From this graph, we can conclude that we are measuring at optical frequencies around the second frequency bands of the 2D photonic crystal. To relate the band structure to our measurements, Figure 4d displays the calculated band structure as a function of wavelength and angle where

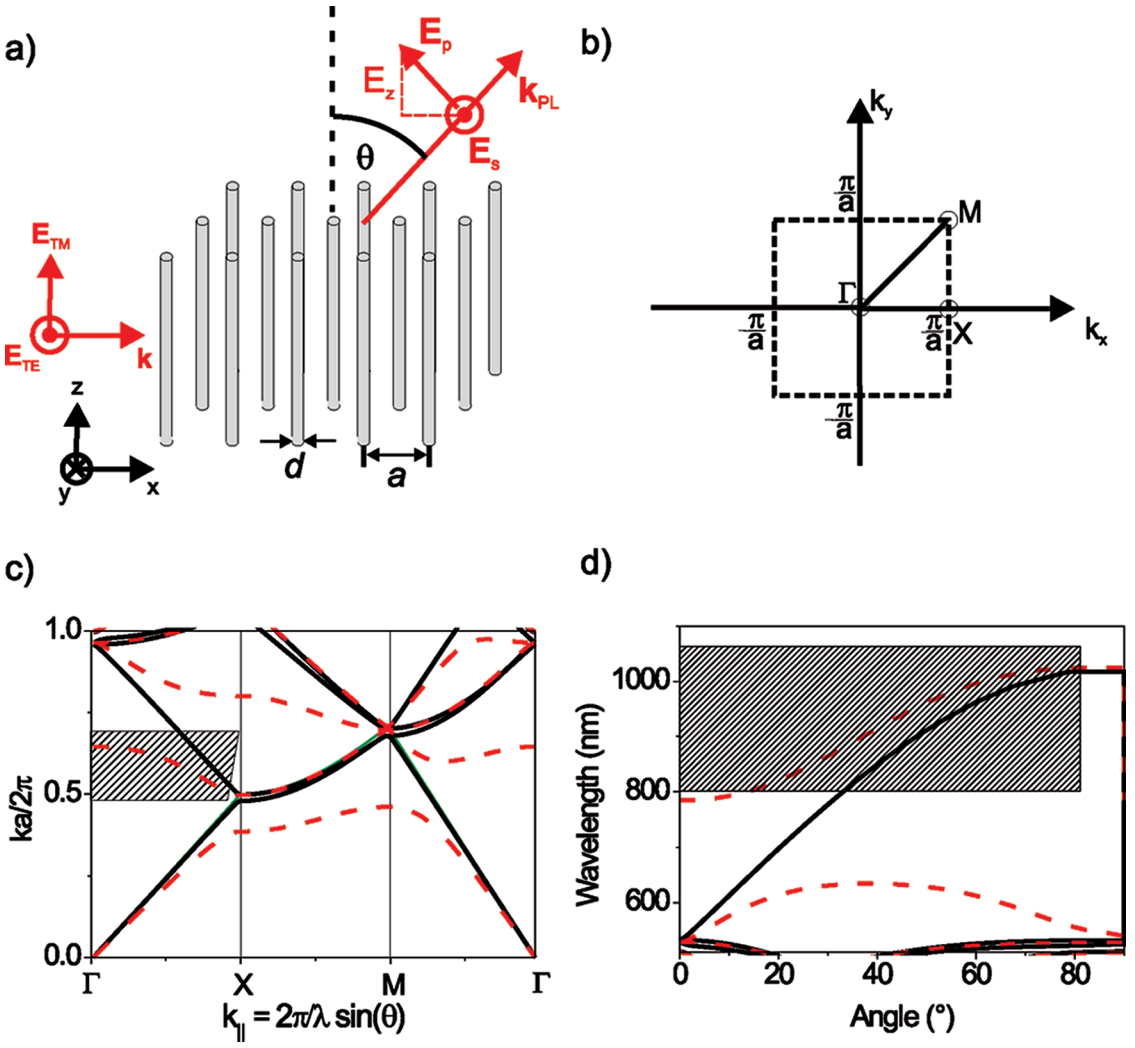

Figure 4. (a) Schematic representation of an array of nanowires. The wavevector of TE and TM modes is displayed, with TE modes having the electric field along the *y*-direction and TM modes having the electric field along the *z*-direction. The lattice constant is *a* and the diameter of the nanowires is *d*. The wavevector of the emission is illustrated, together with the electric field for s- and p-polarized light. (b) Reciprocal lattice of a square array of nanowires. The edges of the irreducible Brillouin zone are the Γ, X, and M points. (c) Calculated band structure of a 2D photonic crystal formed by a square lattice of infinitely long cylinders with refractive index $n = 3.35$, a diameter of 90 nm, and a lattice constant of 510 nm surrounded by air. The black solid curves correspond to TE modes, while the red dashed curves are TM modes. The dashed area corresponds to the range of our measurement. (d) Calculated band structure as a function of wavelength and angle. The dashed area corresponds to the range of our measurement.

the shaded rectangle corresponds to the range of our measurements.

We have included the calculated second frequency bands in the measurements displayed in Figure 3. The white curve in Figure 3a represents the second TE frequency band, and the white curve in Figure 3b corresponds to the second TM frequency band. We find a good agreement between the calculated band structure and the bands of increased emission of the InAsP segment. Also the modulation of the p-polarized nanowire emission at $\lambda = 875$ nm (Figure 3b) can be related to the occurrence of a Bloch mode in the periodic structure and, as we will show later, to Fabry-Pérot resonances due to the finite thickness of the periodic array of nanowire. It is important to point out that the band structure calculations neglect absorption and dispersion of the refractive index. In addition, the finite length of the nanowires limits the validity of the description of this system in terms of a 2D photonic crystal. Nonetheless, the good agreement between the band structure calculation and the photoluminescence indicates the relevance of the periodic structure in the definition of the directional light emission. This agreement justifies the following explanation for the emission of the array: The photoexcited nanowires and InAsP segments decay preferentially into eigenmodes of the periodic structure, which are coupled at the interfaces to free space radiation. Figure 5a illustrates the directionality of the emission of the InAsP segment by plotting the emission at $\lambda = 956$ nm as a function of the angle for s-polarized (open triangles) and p-polarized light (open squares). While the increase of the

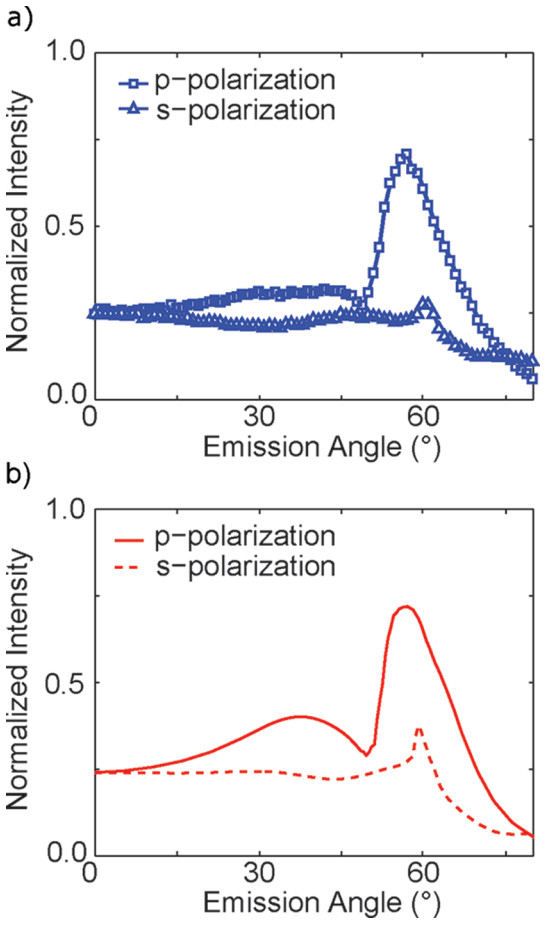

Figure 5. (a) Photoluminescence measurements and (b) FDTD simulations at λ = 950 nm of InAsP segments in InP nanowires organized in a periodic array as a function of the emission angle. The data are normalized to the maximum emission at 875 nm. The open squares and triangles in panel a corresponds to p-polarized emission and s-polarized emission, respectively, while the solid and dashed lines in panel b are the simulations for p- and s-polarized emissions.

emission for s-polarized light at 59° is small, the emission of p-polarized light is strongly directed at 56°. This difference in intensity between the s- and p-polarized light is due to the different field profiles of the TE and TM modes. Calculations of the field profiles (not shown here) show that while the electrical energy density in the TE mode is the strongest in the air surrounding the nanowires, the electrical energy density in the TM mode is concentrated in the nanowires. Therefore, the light emitted from the active region of the samples, that is, from the nanowires and InAsP segments can couple more efficiently to the TM mode, which is coupled to s-polarized light into free space at the sample interface.

We have performed finite-difference time-domain (FDTD) simulations to simulate the emission of heterostructured InP−InAsP−InP nanowires with a height of 3 μm, a straight top part, and a tapered base ordered in a square lattice with a constant of 510 nm. We have used an in-house developed FDTD program on a computational domain consisting of a nanowire on a semi-infinite substrate.[27] To simulate the periodic structure, the domain has quasiperiodic boundary conditions in the horizontal directions and absorbing perfectly matched layers (PML) in the vertical directions. A continuous function describing the dispersion of the permittivity of InP is obtained by fitting the refractive index of InP with a Lorentz model above and below the bandgap.[28] The intensity radiated by any distribution of incoherent dipoles in the nanowire can be efficiently calculated by invoking the reciprocity theorem.[29] With this theorem the radiated intensity in a specific direction and polarization is computed by evaluating the near field at the emitting segment caused by an incident field. By illuminating the nanowire structure with a short broadband pulse, the entire wavelength range can be simulated at once per horizontal wavenumber or angle of incidence. This simulation of the near field is repeated for each angle of incidence. By the reciprocity theorem, the emission intensity in a certain direction and polarization caused by the emission of incoherent dipoles in the emitting segment is proportional to the integrated near-field intensity in the emitting segment that results from the illumination with a polarized plane wave incident from this direction. Using the reciprocity theorem, the local radiative density of states in the photonic crystal can be determined. This radiative density of states contains the extraction efficiency of the emission and the local density of states given by the periodic structure. The reciprocity theorem does not allow determining the local density of states alone.

Initially, we assume that the strength of the radiating dipoles in the wires is independent of position and emission wavelength. To obtain the radiation spectrum that can be compared to experimental data, the dipole strength in the emitting segment is multiplied by the spectral emission of the InAsP segment. This emission is obtained from the photoluminescence measurement of a single nanowire (see Figure 2d) and is a Lorentzian function centered at λ = 956 nm and with a width of 60 nm. Similarly, the emission from the InP nanowire is computed by integrating the radiation from the near field inside the wire and multiplying this to a spectral emission of wurtzite InP. Similarly, this emission is obtained from the photoluminescence measurement of a single nanowire and is a Lorentzian function centered at λ = 875 nm and with a width of 40 nm (see Figure 2d). In all these simulations we take into account the inhomogeneous absorption of the light used for the excitation by multiplying the radiated intensity with a linear function that goes from zero to one from the bottom to the top of the nanowire layer. This distribution of intensities is justified by the recent demonstration of the enhanced absorption in similar arrays of nanowires.[24]

Figure 6 panels a and b show contour plots of the normalized simulated intensity of the array of nanowires for s- (Figure 6a) and p- (Figure 6b) polarization as a

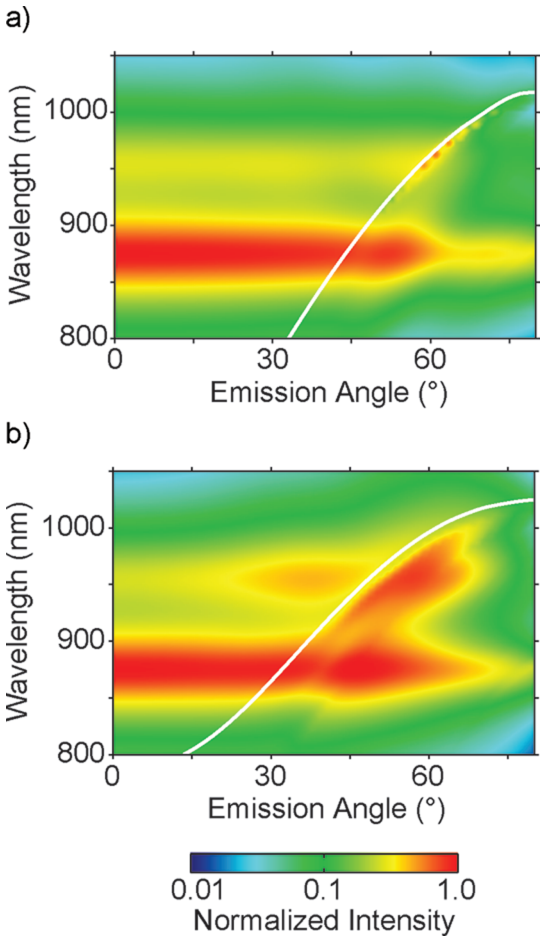

Figure 6. FDTD simulation of the s-polarized (a) and p-polarized (b) photoluminescence of arrays of InP nanowires as a function of the emission angle and wavelength. The white curves correspond to the calculated (a) TE and (b) TM Bloch modes.

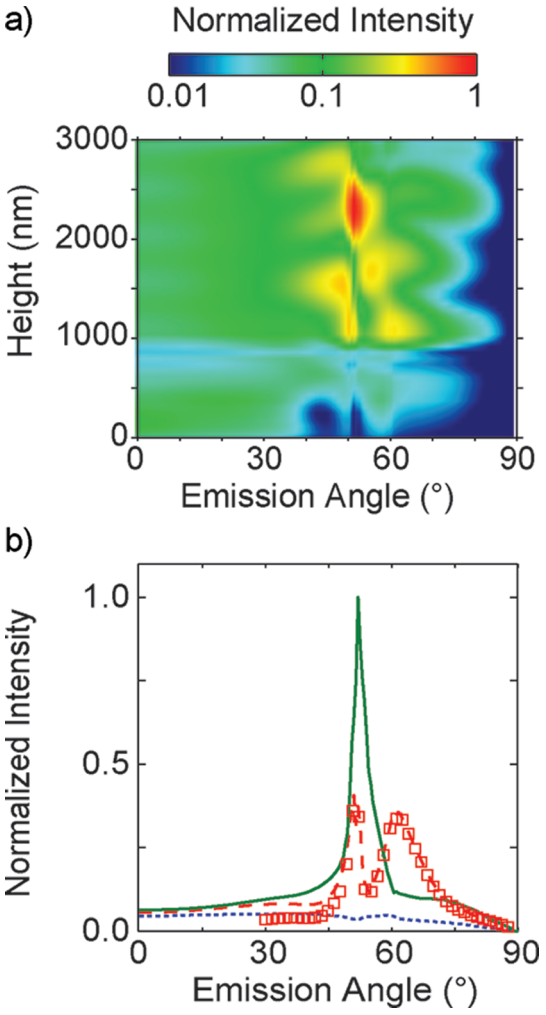

Figure 7. Emission at λ = 956 nm of an array of InP nanowires normalized to the maximum as a function of the emission angle and the vertical position of an InAsP emitting segment of 20 nm embedded in the nanowires. This emitting segment is assumed to be formed by incoherent and randomly oriented dipoles. In this simulation, we do not take into account the inhomogeneous absorption of the light in the nanowire layer. (a) Corresponds to the emission of p-polarized light. (b) Normalized emission intensity of p-polarized light for three different heights of the InAsP segments: h = 540 nm (dotted line), 1080 nm (dashed line), and 2220 nm (solid line). The squares indicate the emission intensity from a height of 1080 nm of vertically aligned dipoles.

function of wavelength and angle of emission. In the FDTD simulation, we assume a random and isotropic distribution of emitting dipoles in the nanowires, and the InAsP segment is located at a height of 1920−1940 nm. The simulations show a remarkable good agreement with the measurements of Figure 3. This agreement can be better appreciated in the cuts to the contour plots at λ = 956 nm displayed in Figure 5b. In this figure the solid curve represents the p-polarized emission, while the dashed curve is the s-polarized emission. The good agreement between measurements and simulations shows that the gold particle on top of the nanowires, which is not included in the FDTD simulations, does not influence the directionality of the emission. This independence of the emission on the presence of the gold particles might be due to its high InP contamination, that is inevitable in the VLS method used for growing the nanowires. The InP-gold alloy is expected to have a weaker effect on the optical properties of nanowires than intrinsic gold.

The good agreement between measurements and FDTD simulations motivates us to determine the influence of the vertical position of the emitting segment on the direction of the emission. Figure 7a shows the simulated p-polarized photoluminescence at λ = 956 nm. To take account for the tapering of the nanowire, this simulated photoluminescence is normalized to the area of the emitting segment in the wire and normalized to the maximum emission as a function of the detector angle and the vertical position of the emitting segment in the nanowire. The photoluminescence exhibits maxima around 50° corresponding to the TM mode. However, the local radiative density of states causes a strong dependence of the direction and of the efficiency of the photoluminescence on the vertical

position of the emitting segment.[30] This influence of the height of the emitting segment on the far-field emission is illustrated in Figure 7b, where cuts to the contour plot are presented for three different heights, namely, h = 540 nm (dotted curve), h = 1080 nm (dashed curve), and h = 2220 nm (solid curve). Note that for h = 540 nm the emitting segment is located in the tapered bottom part of the nanowires, where the emitted radiation can couple efficiently to guided modes in the nanowire and transmit efficiently into the substrate, leading to a very low emission. This enhanced coupling of light into the substrate has been recently experimentally demonstrated.[24] For h = 1080 nm there are two peaks at 46° and 57°, which both can be related to the TM mode. For the band calculations of the infinitely long 2D photonic crystal we have assumed the vertical component of the wave vector to be zero, leading to a single eigenfrequency per incident angle. In a photonic crystal slab, such as the nanowire array, the z-component of the wavevector inside the slab can be nonzero, resulting in a broad continuum of TM-like modes. The exact shape of the emission from this continuum is given by the local radiating density of states and is influenced by a vertical Fabry–Pérot resonance in the slab and the coupling of the z-component of the wavevector of the mode with that of the emitted field in air.[31] To demonstrate that the features of the p-polarized emission are indeed only influenced by the TM-like modes and the Fabry–Pérot resonance in the nanowire layer, we have simulated the p-polarized emission of the array of nanowires for dipoles that are either horizontally or vertically oriented, separately. Vertically oriented dipoles can only couple to TM modes and horizontally oriented dipoles to TE modes. The squares in Figure 7b represent the simulated emission of vertically oriented dipoles at h = 1080 nm. This emission overlaps the simulation done by considering a random distribution of emitting dipoles (red dashed curve). We can conclude that the emission of the emitting segment is mainly caused by vertically oriented dipoles that couple to the TM-like photonic crystal slab mode and the contribution of the emission of horizontally oriented dipoles, that couple to TE-like modes, on the p-polarized emission is negligible. In the case of h = 2220 nm there is only one pronounced peak at 48°. This peak is 3.5 times higher than the peak found for the InAsP segment in the measured sample (h = 1920 nm). The simulations show a strong tunability of the directionality and the efficiency of the emission by the vertical position of the emitting segment.

CONCLUSION

We have demonstrated the modified emission of heterostructures embedded in ordered arrays of semiconductor nanowires. From calculations of the Bloch modes supported by 2D photonic crystals, we conclude that the periodic structure determines the directionality of the emission. Finite-difference time-domain simulations for an isotropic distribution of emitting dipoles reproduce the measurements. The simulations reveal a strong influence of the position of the emitting segment in the nanowires on the emission efficiency and direction. These results set the base for the design of the emission of nanowire-based LEDs and single-photon sources based on photonic crystals of semiconductor nanowires.

METHODS

VLS growth: Heterostructured InP–InAsP–InP nanowires are grown for 60 min at a temperature of 420 °C using trimethylindium (TMIn) and phosphine (PH_3) as precursors. After 30 min of InP growth, the InAsP segment is grown by adding arsine (AsH_3) for 10 s into the MOVPE reactor.

Angle-resolved photoluminescence measurements: The fiber of a fiber-coupled InGaAs spectrometer was mounted on a computer-controlled rotational stage, and the fiber was rotated around the nanowire sample. The excitation source was a diode laser emitting at a wavelength of 532 nm. The laser light was incident onto the sample at an angle of 60° with respect to the surface normal. The measurements were performed at room-temperature.

Acknowledgment. We thank G. Immink for the growth of the nanowires, E. van Thiel, M. Verschuuren, E. Timmering, and R. van de Laar for technical assistance, F. Holthuysen for SEM analysis, M. Verheijen for TEM analysis, and M. Leistikow and W. Vos for useful discussions. This work is part of the research program of the "Stichting voor Fundamenteel Onderzoek der Materie (FOM)", which is financially supported by the "Nederlandse organisatie voor Wetenschappelijk Onderzoek (NWO)" and is part of an industrial partnership program between Philips and FOM. This research is supported by the Dutch Technology Foundation STW, which is the applied science division of NWO, and the Technology Programme of the Ministry of Economic Affairs (Project No. 10301).

REFERENCES AND NOTES

1. Lee, K. G.; Chen, X. W.; Eghlidi, H.; Kukura, P.; Lettow, R.; Renn, A.; Sandoghdar, V.; Götzinger, S. A Planar Dielectric Antenna for Directional Single-Photon Emission and Near-Unity Collection Efficiency. *Nat. Photonics* **2011**, *5*, 166–169.
2. Vecchi, G.; Giannini, V.; Rivas, J. G. Shaping the Fluorescent Emission by Lattice Resonances in Plasmonic Crystals of Nanoantennas. *Phys. Rev. Lett.* **2009**, *102*, 146807.
3. Ogawa, S.; Imaga, M.; Yoshimoto, S.; Okano, M.; Noda, S. Control of Light Emission by 3D Photonic Crystals. *Science* **2004**, *305*, 226–229.
4. Bergenek, K.; Wiesmann, C.; Zull, H.; Wirth, R.; Sundgren, P.; Linder, N.; Streubel, K.; Krauss, T. F. Directional Light Extraction from Thin-Film Resonant Cavity Light-Emitting Diodes with a Photonic Crystal. *Appl. Phys. Lett.* **2008**, *93*, 231109.
5. Wierer, J. J.; David, A.; Megens, M. M. III-Nitride Photonic-Crystal Light-Emitting Diodes with High Extraction Efficiency. *Nat. Photonics* **2009**, *3*, 163–169.

6. Rangel, E.; Matioli, E.; Choi, Y.-S.; Weisbuch, C.; Speck, J. S.; Hu, E. L. Directionality Control Through Selective Excitation of Low-Order Guided Modes in Thin-Film InGaN Photonic Crystal Light-Emitting Diodes. *Appl. Phys. Lett.* **2011**, *98*, 081104.
7. Huang, M. H.; Mao, S.; Feick, H.; Yan, H.; Wu, Y.; Kind, H.; Weber, E.; Russo, R.; Yang, P. Room-Temperature Ultraviolet Nanowire Nanolasers. *Science* **2001**, *292*, 1897.
8. Minot, E. D.; Kelkensberg, F.; van Kouwen, M.; van Dam, J. A.; Kouwenhoven, L. P.; Zwiller, V.; Borgström, M. T.; Wunnicke, O.; Verheijen, M. A.; Bakkers, E. P. A. M. Single Quantum Dot Nanowire LEDs. *Nano Lett.* **2007**, *7*, 367–371.
9. Claudon, J.; Bleuse, J.; Malik, N.; Bazin, M.; Jaffrennou, P.; Gregersen, N.; Sauvan, C.; Lalanne, P.; Gérard, J. A Highly Efficient Single-Photon Source Based on a Quantum Dot in a Photonic Nanowire. *Nat. Photonics* **2010**, *4*, 174–177.
10. Wagner, R. S.; Ellis, W. C. Vapor—Liquid—Solid Mechanism of Single Crystal Growth. *Appl. Phys. Lett.* **1964**, *4*, 89–90.
11. Haraguchi, K.; Katsuyama, T.; Hiruma, K.; Ogawa, K. GaAs p-n Junction Formed in Quantum Wire Crystals. *Appl. Phys. Lett.* **1992**, *60*, 745–747.
12. Stiegler, J. M.; Huber, A. J.; Diedenhofen, S. L.; Rivas, J. G.; Algra, R. E.; Bakkers, E. P. A. M.; Hillenbrand, R. Nanoscale Free-Carrier Profiling of Individual Semiconductor Nanowires by Infrared Near-Field Nanoscopy. *Nano Lett.* **2010**, *10*, 1387–92.
13. Lauhon, L. J.; Gudiksen, M. S.; Wang, D.; Lieber, C. M. Epitaxial Core—Shell and Core—Multishell Nanowire Heterostructures. *Nature* **2002**, *420*, 57.
14. Bakkers, E. P. A. M.; van Dam, J. A.; Franceschi, S. D.; Kouwenhoven, L. P.; Kaiser, M.; Verheijen, M.; Wondergem, H.; van der Sluis, P. Epitaxial Growth of InP Nanowires on Germanium. *Nat. Mat.* **2004**, *3*, 769–773.
15. Borgström, M. T.; Zwiller, V.; Müller, E.; Imamoglu, A. Optically Bright Quantum Dots in Single Nanowires. *Nano Lett.* **2005**, *5*, 1439–1443.
16. Mårtensson, T.; Svensson, C. P. T.; Wacaser, B. A.; Larsson, M. W.; Seifert, W.; Deppert, K.; Gustafsson, A.; Wallenberg, L. R.; Samuelson, L. Epitaxial III/V Nanowires on Silicon. *Nano Lett.* **2004**, *4*, 1987–1990.
17. Mårtensson, T.; Borgström, M. T.; Seifert, W.; Ohlsson, B. J.; Samuelson, L. Fabrication of Individually Seeded Nanowire Arrays by Vapour—Liquid—Solid Growth. *Nanotechnolgy* **2003**, *14*, 1255–1258.
18. Jensen, L. E.; Björk, M. T.; Jeppesen, S.; Persson, A. I.; Ohlsson, B. J.; Samuelson, L. Role of Surface Diffusion in Chemical Beam Epitaxy of InAs Nanowires. *Nano Lett.* **2004**, *4*, 1961–1964.
19. Mohan, P.; Motohisa, J.; Fukui, T. Controlled Growth of Highly Uniform, Axial/Radial Direction-defined, Individually Addressable InP Nanowire Arrays. *Nanotechnology* **2005**, *16*, 2903–2907.
20. Fan, H. J.; Lee, W.; Scholz, R.; Dadgar, A.; Krost, A.; Nielsch, K.; Zacharias, M. Arrays of Vertically Aligned and Hexagonally Arranged ZnO Nanowires: A New Template-Directed Approach. *Nanotechnology* **2005**, *16*, 913.
21. Fan, H. J.; Fuhrmann, B.; Scholz, R.; Syrowatka, F.; Dadgar, A.; Krost, A.; Zacharias, M. Well-Ordered ZnO Nanowire Arrays on GaN Substrate Fabricated *via* Nanosphere Lithography. *J. Cryst. Growth* **2006**, *287*, 34–38.
22. Pierret, A.; Hocevar, M.; Diedenhofen, S. L.; Algra, R. E.; Vlieg, E.; Timmering, E. C.; Verschuuren, M. A.; Immink, G. W. G.; Verheijen, M. A.; Bakkers, E. P. A. M. Generic Nano-Imprint Process for Fabrication of Nanowire Arrays. *Nanotechnology* **2010**, *21*, 065305.
23. Verschuuren, M.; Wuister, S. Imprint lithography. US 2008/0011934 2008.
24. Diedenhofen, S. L.; Janssen, O. T.; Grzela, G.; Bakkers, E. P. A. M.; Gómez Rivas, J. Strong Geometrical Dependence of the Absorption of Light in Arrays of Semiconductor Nanowires. *ACS Nano* **2011**, *5*, 2316–2323.
25. Mattila, M.; Hakkarainen, T.; Mulot, M.; Lipsanen, H. Crystal-Structure-Dependent Photoluminescence from InP Nanowires. *Nanotechnology* **2006**, *17*, 1580.
26. Johnson, S. G.; Joannopoulos, J. D. Block-iterative Frequency-Domain Methods for Maxwell's Equations in a Planewave Basis. *Opt. Express* **2001**, *8*, 173–190.
27. Lalanne, P.; Besbes, M.; Hugonin, J. P.; van Haver, S.; Janssen, O. T. A.; Nugrowati, A. M.; Xu, M.; Pereira, S. F.; Urbach, H. P.; van de Nes, A. S.; et al. Numerical Analysis of a Slit-Groove Diffraction Problem. *J. Eur. Opt. Soc., Rapid Publ.* **2007**, *2*, 07022.
28. Palik, E., Ed. *Handbook of Optical Constants of Solids*; Academic Press, San Diego, CA, 1998.
29. Janssen, O. T. A.; Wachters, A. J. H.; Urbach, H. P. Efficient Optimization Method for the Light Extraction from Periodically Modulated LEDs Using Reciprocity. *Opt. Express* **2010**, *18*, 24522–24535.
30. Koenderink, A. F.; Kafesaki, M.; Soukoulis, C. M.; Sandoghdar, V. Spontaneous Emission in the Near Field of Two-Dimensional Photonic crystals. *Opt. Lett.* **2005**, *30*, 3210–2.
31. David, A.; Benisty, H.; Weisbuch, C. Spontaneous Emission in GaN/InGaN Photonic Crystal Nanopillars. *Opt. Express* **2007**, *15*, 17991.